2008 IEEE International Conference on
Robotics and Automation
Pasadena, CA, USA, May 19-23, 2008

A Microrobotic Adherent Cell Injection System for Investigating Intracellular Behavior of Quantum Dots

W.H. Wang*, *Member, IEEE,* Y. Sun*, *Senior Member, IEEE,* M. Zhang, R. Anderson, L. Langille and W. Chan

***Abstract*— This paper presents a semi-automated microrobotic system for adherent cell injection. Different from embryos/oocytes that have a spherical shape and regular morphology, adherent cells are flat with a thickness of a few micrometers and are highly irregular in morphology. Based on computer vision microscopy and motion control, the system coordinately controls a three-degrees-of-freedom microrobot and a precision XY stage. The microrobotic system demonstrates an injection speed of 25 endothelial cells per minute with a survival rate of 96% and a success rate of 82% (n=1012). The system has a high degree of performance consistency. It is immune to operator proficiency variations and from human fatigue, requiring a human operator to select injection destinations through computer mouse clicking as the only operator intervention. The microrobotic adherent cell injection system makes the injection of thousands of adherent cells practical and will enable our testing of intracellular behavior of semiconductive quantum dots (QDs).**

***Index Terms*— Adherent cell, microrobotic injection, endothelial cells, quantum dots, molecule screening.**

I. Introduction

Nanoparticles have gained significant interests in biomedical applications (e.g., targeted drug delivery and biomarkers). Their nanometer size is comparable to that of biological molecules, and they can be surface functionalized for targeted conjugation to manipulate or detect biological structures at the molecular and cellular levels. *In vitro* investigation of intracellular behavior of nanoparticles has important implications in nanotoxicity, intracellular imaging, drug delivery, therapeutics, and the design of multifunctional nanoparticles [1], [2], [3]. Among many types of nanoparticles, semiconductive quantum dots (QDs) are widely used [4] due to desired optical properties such as narrow fluorescence emission and stability against photobleaching.

In previous studies, incubation of cells with silica-coated QDs caused nanoparticles to be trapped in vesicles [5], hampering the investigation of how differently coated QDs interact with intracellular organelles. Thus, we changed the approach to direct injection of CdSe/ZnS QDs into cytoplasm, which would circumvent transportation barriers. Our experimental design involves five common types of coatings (bifunctionalized ligand, silanization, hydrophobic interaction, amphiphilic polymer, and hydroxylated [4]) to target six potential organelle candidates including mitochondria, centrosome, golgi, lysosome, vacuole and ribosome. In order to obtain statistically significant biological data and determine whether each coating aggregates around a specific intracellular organelle in a targeted manner, each combination would require the injection of a minimum of 1,000 mammalian cells, amounting to a total of 30,000 cells.

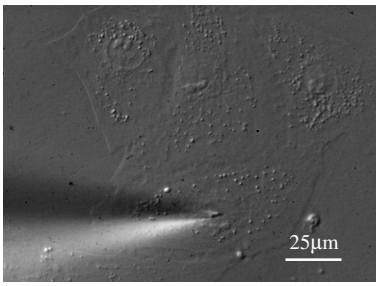

Fig. 1. Injection of endothelial cells that are 3.8-5.5μm thick.

Leveraging microrobotics, it would become practical to inject tens of thousands of adherent cells within a reasonable time window, which is not feasible for manual operation due to the slow speed, human fatigue, low reproducibility, and low success rates [6]. Efforts from many researchers for automating cell injection have been continuous. The vast majority of these systems [7], [8], [9], [10], [11], [12], [13] were developed to facilitate the handling of mouse/*Drosophila*/zebrafish embryos/oocytes for transgenetics and reproduction applications.

In microrobotic injection of suspended cells (e.g., embryos/oocytes), cells must be immobilized, preferably into a regular pattern to minimize cell searching and switching tasks and increase injection speed [13]. Differently, most mammalian cells (e.g., HeLa cells, fibroblasts, and endothelial cells) adhere to the bottom surface of a culture dish/plate during *in vitro* culture [14]. Although adherent cells do not require immobilization efforts, they are highly irregular in morphology (Fig. 1), which makes robust pattern recognition difficult and full automation challenging. Additionally, they are only a few micrometers thick, posing more stringent requirements in microrobotic positioning.

Wang is with Dept. of Mechanical Engineering, University of Canterbury, Private Bag 4800, Christchurch 8140, New Zealand (e-mail: wenhui.wang@canterbury.ac.nz).

Sun is with the Advanced Micro and Nanosystems Laboratory, University of Toronto, 5 King's College Road, Toronto, ON, Canada, M5S 3G8 (e-mail: sun@mie.utoronto.ca).

Zhang and Langille are with Division of Cellular and Molecular Biology, Toronto General Research Institute, 101 College Street, Toronto, ON, Canada, M5G 1L7.

Anderson and Chan are with Institute of Biomaterials and Biomedical Engineering, University of Toronto, Rosebrugh Building, 164 College Street, Toronto, ON, Canada, M5S 3G9.

978-1-4244-1647-9/08/$25.00 ©2008 IEEE.

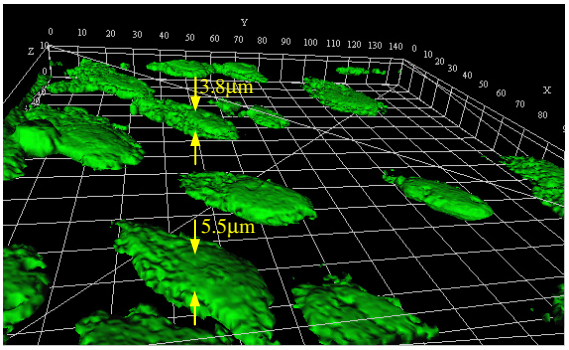

Fig. 2. 3-D profile of endothelial cells. Reconstructed from a stack of confocal fluorescence images.

Adherent cell injection is not only relevant to our current intracellular QD study, but also important in general molecule screening and cellular response testing [15], [16], [17]. As one of the mammalian adherent cell types, endothelial cells were chosen for our intracellular QD study. Endothelial cells line the entire circulatory system from the heart to the smallest capillary, playing important roles in the vascular system.

Fig. 2 shows a 3D profile of endothelial cells reconstructed from a stack of confocal fluorescence images. Cells cultured on the bottom of a Petri dish are flat with a thickness varying from 3.8μm to 5.5μm. The small thickness and large variations require accurate determination of relative vertical positions between the injection micropipette and a cell. For detecting micropipette-cell contact, a previously reported method employed electrodes inside the injection micropipette and culture dish [18]. Detection is conducted through monitoring impedance changes. Factors that could induce detection errors are type and concentration of cell medium and injection solution.

To tackle the problem of relative vertical position determination, the contact detection method used in our microrobotic adherent cell injection system is computer vision microscopy based [19] without requiring additional sensors. The contact detection method demonstrates an accuracy of 0.2μm.

The microrobotic system presented in this paper operates semi-automatically. To overcome the remained human intervention towards fully automated adherent cell injection, robust image processing algorithms for recognizing highly irregular cell structures must be developed to enable the system to automatically determine deposition destinations, which are currently selected by a human operator.

II. System Design

A. System Setup

The system, shown in Fig. 3, employs a three-degrees-of-freedom microrobot (MP-285, Sutter) with a travel of 25mm and a 0.04μm positioning resolution along each axis. One motion control card (NI PCI-6289) is mounted on a host computer (3.0GHz CPU, 1GB memory) where control algorithms operate. Visual feedback is obtained through a

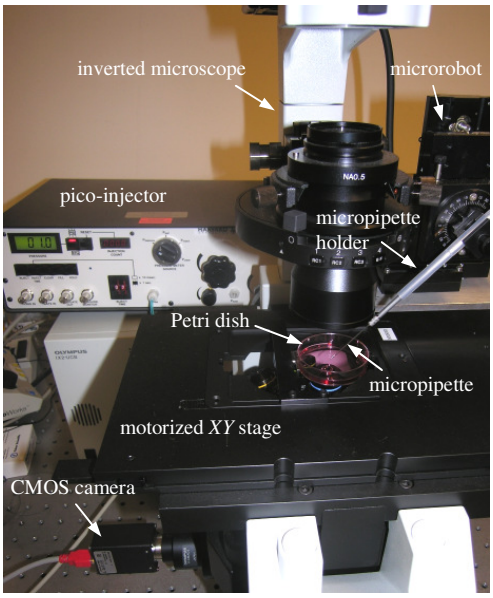

Fig. 3. Microrobotic system for adherent cell injection.

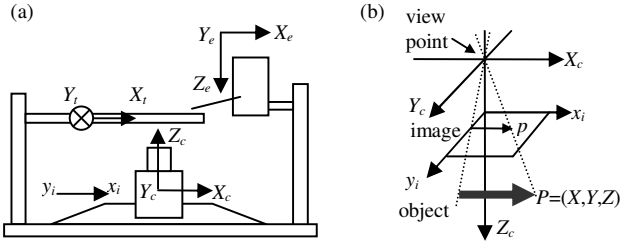

Fig. 4. (a) Coordinate frames of the system. (b) Image projection model relating the camera coordinate frame to the image plane.

CMOS camera (A601f, Basler) mounted on an inverted microscope (IX81, Olympus). A Polystyrene Petri dish (55mm, Falcon) where the endothelial cells are seeded is placed on a motorized precision XY stage (ProScanII, Prior). A glass micropipette, heated and pulled using a micropipette puller (P-97, Sutter), is connected to the microrobot via a micropipette holder. The micropipette is tilted 45°C with respect to the XY stage. A computer-controlled pico-injector (PLI-100, Harvard Apparatus) with a femto-liter resolution provides positive pressure for material deposition. All units except the host computer and pressure unit are placed on a vibration isolation table.

The coordinate frames of the system defined in Fig. 4(a) are summarized in Table I. A point P=(X, Y, Z) in the camera frame c is mapped to a point p=(u, v) in the image plane i via a scaled orthographic projection (Fig. 4(b)).

B. Micropipette Processing

Injection of mammalian adherent cells requires the use of injection micropipettes with a tip of 0.1 to 1μm in outer diameter in order to minimize cell damage and warrant a high survival rate. Many micropipette processing parameter combinations were tested. SEM (scanning electron microscopy) was used to accurately measure the inner diameter (ID) and

TABLE I

SUMMARY OF COORDINATE FRAMES

Symbol	Coordinate frame
e	End-effector coordinate frame X_e-Y_e-Z_e attached to microrobot that controls the motion of the injection micropipette
t	Target coordinate frame X_t-Y_t-Z_t attached to motorized XY stage that controls the motion of cells
c	Camera coordinate frame X_c-Y_c-Z_c
i	Image plane x_i-y_i (or x-y)

TABLE II

PULLED MICROPIPETTE TIP SIZE UNDER VARIOUS PULLER SETTINGS †

Heat	Pull	Vel	Time	Pressure	OD/ID (μm)
500	60	60	250	300	0.54/0.27
500	58	60	250	300	0.67/0.35
500	60	50	250	300	0.68/0.35
500	55	60	250	300	0.73/0.4
500	58	50	250	300	0.87/0.6
500	55	50	250	300	1.28/0.9
500	50	50	250	300	1.69/1.21

† Micropipette pulling parameters. Ramp value: 479. Starting glass tubing: OD/ID = 1.0/0.78mm.

outer diameter (OD) of pulled micropipettes. Table II summarizes selected sets of processing parameters and resulting micropipette tip sizes.

With a tip of OD/ID=0.54/0.27μm or smaller, QDs rapidly aggregated at the tip end and cause clogging, as shown in Fig. 5(a). In this study, micropipette tips with an OD/ID of 0.87/0.6μm were selected since clogging is greatly suppressed and cell damage is insignificant. Fig. 5(b) shows an SEM image of a micropipette tip with OD/ID of 0.87/0.6μm.

C. Injection Volume Control

Volume of foreign materials inserted into a cell should not exceed 5% of the cell's cytoplasmic volume. Volume calibration is also critical for precisely depositing a specified amount of materials into individual cells such that dose effect can be investigated. Deionized (DI) water is used as an example in this section to describe the calibration of the relationship between injection volume, applied pressure, and pressure 'on' time (i.e., pulse length). A drop of DI water pushed out of the injection micropipette forms a sphere at the micropipette tip, which is immersed into a drop of mineral oil. Injection volume is then calculated by detecting the diameter of the sphere via a Hough transform.

For a micropipette tip of OD/ID=0.87/0.6μm, Fig. 6 shows the relationship of injected volume vs. pressure pulse length, corresponding to an injection pressure level of 40psi.

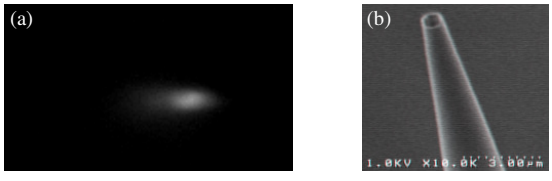

Fig. 5. (a) QDs cause micropipette tip clogging (OD/ID=0.54/0.27μm), indicated by the bright spot in tip's close vicinity. QDs were coated with 40% octadecylamine modified poly(acrylic acid). (b) SEM image of a pulled tip with OD/ID=0.87/0.6μm.

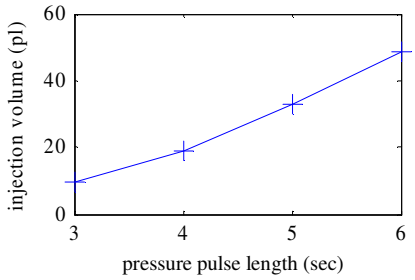

Fig. 6. Injection volume calibration by visually measuring dispensed droplet sizes through Hough transform.

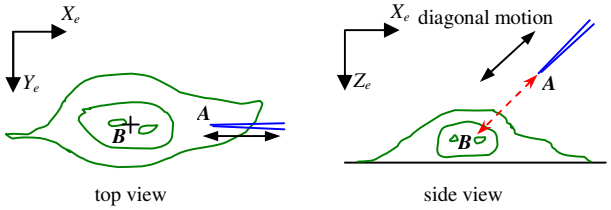

Fig. 7. The injection micropipette tip moves along the diagonal direction from its initial position A to the selected destination B for material deposition. A and B are chosen to be 8μm and 3μm above Petri dish surface.

Droplets smaller than 10pl cannot be accurately quantified through visual measurements. By controlling the pressure level and pressure pulse length, $\sim$1fl (femto-liter) material was deposited into each endothelial cell in the experiments with a high reproducibility.

III. CONTACT DETECTION

In order to deposit materials within a cell (Fig. 7), the relative vertical positions of the micropipette tip and the Petri dish surface along the Z_e direction must be accurately known before injection starts. As operation speed and robustness are prioritized, low complexity in system setup is highly desirable. Without the inclusion of an extra sensor (e.g., touch or force sensor), a computer vision-based contact detection technique was developed [19] for accurately determining the relative heights of the micropipette tip (controlled by the microrobot) and the surface of the Petri dish where the cells are seeded.

For contact detection, the micropipette first moves only along the Y_e direction to identify the micropipette tip. Upon identification, the x- and y-coordinates in the image plane i and the X_e- and Y_e-coordinates of the micropipette tip in the end-effector frame e are determined and used to establish the transformation between the image frame and the X_e-Y_e plane.

After the identification of the micropipette tip, the micropipette moves only along the vertical direction (Z_e) to establish contact with the surface. After the establishment of contact in the world frame, further vertical motion of the micropipette tip induces horizontal motion in the image plane. Before and after contact, the x-coordinates of the micropipette tip in the image plane i result in a V-shaped curve. Searching for the global minimum locates the peak of

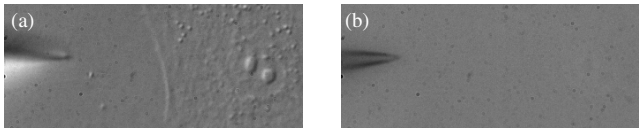

Fig. 8. (a) Under phase contrast (40×). (b) Under bright field (40×).

the curve that represents the contact position. The entire contact detection process completes between 6-10s, achieving an accuracy of 0.2μm. Under a high magnification of 40×, the microrobot speed was controlled not to exceed 1μm/sec in order to avoid micropipette breakage, which is limited by the speed of image processing.

Although phase contrast or DIC (differential interference contrast) produces desired visualization effects (pseudo-3D view of cells) for cell imaging (Fig. 8(a)), due to the small micropipette tip size, it was found in experiments that the bright-field imaging mode is more favorable for contact detection. Under bright field, the tip pattern is more uniform and 'halo' free (Fig. 8(b)), resulting in more reliable tracking and better reproducibility in contact detection.

With the initial contact between the micropipette tip and the Petri dish surface accurately determined, the microrobot moves upwards by 8μm above the contact position, which is slightly greater than the cell height ($\sim$5μm) to prevent possible crashing with a cell when switching from one cell to the next. The Z_e-coordinate of injection destination for material deposition was set at 3μm above the contact position.

For a sub-micrometer-sized micropipette tip, clogging due to cell debris accumulation and impurity of injection materials is unavoidable. Micropipette tips with OD/ID of 0.87/0.6μm used in the experiments typically became clogged after injecting 50 endothelial cells. Every micropipette exchange requires the redetermination of relative vertical positions of the micropipette tip and Petri dish surface, which is greatly facilitated by the automated contact detection technique.

IV. Microrobotic Adherent Cell Injection

A. Overall Sequence

A Petri dish with cells seeded is placed on the motorized *XY* stage. Injection starts with vision-based contact detection to automatically determine the vertical positions of the micropipette tip and the surface of the Petri dish (Fig. 9). For all cells within the field of view, a human operator selects deposition destinations by computer mouse clicking in the control program interface. Based on the operator input coordinates in the image plane, the system determines the shortest injection path, according to which the micropipette tip moves to a cell, penetrates the cell membrane, deposits the specified volume of materials, retracts out of the cell, moves upwards by 8μm above the contact position, and then switches to the next cell for injection.

After all cells within the field of view are injected, the precision *XY* stage positions the Petri dish to bring the next segment of cells into the field of view. The injection process is repeated until all cells in desired segments of the Petri dish are injected. During system operation, although the Petri dish is 2D positioned by the *XY* stage, the microrobot is servoed along three axes. PID (proportional-integral-derivative) control is employed for positioning both the microrobot and the *XY* stage.

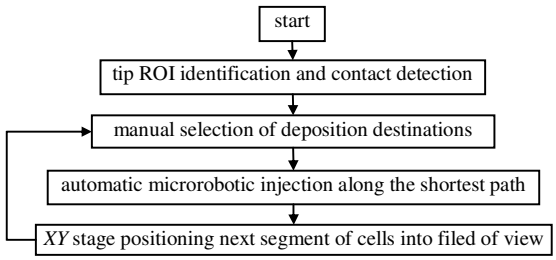

Fig. 9. Control flow of semi-automated microrobotic adherent cell injection.

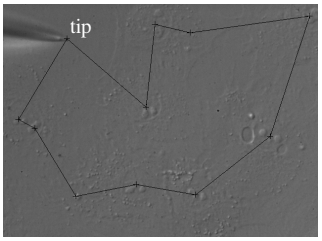

Fig. 10. Injection path. '+' represents a user selected injection destination. The system generates the shortest path.

B. Injection Path Optimization

In a random order, the human operator selects *x*- and *y*-coordinates in the image plane as injection destinations for all cells within the field of view. The system employs the classical traveling salesman algorithm [20] to generate the shortest path (Fig. 10), which costs $\sim$0.1sec for computation as each field of view contains only $\sim$10 cells. Note that the injection sequence can either be clockwise or counter-clockwise. Accumulative time savings of injecting 1000 cells by operating along the shortest path can be significant.

C. Microrobotic Control

Motion control of the microrobot is based on position feedback of the microrobot (Fig. 11) according to the PID control law. The transformation between x- and y-coordinates in the image plane *i* and the X_e- and Y_e-coordinates of the micropipette tip in the end-effector frame *e* is established during contact detection (Section III) without requiring an off-line process. From operator input image coordinates, the lateral components of target position P_d for the micropipette tip are thus determined for each cell. Based on the confocal microscopy measured heights of endothelial cells, the vertical component of target position P_d was set at 3μm above the contact position (i.e., Petri dish bottom surface) for all cells. The micropipette penetrates the membrane of a cell and retracts out of the cell both along the diagonal direction, as shown in Fig. 7.

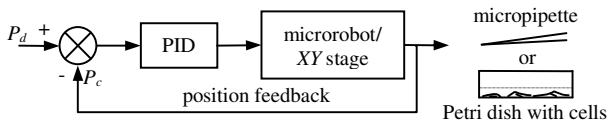

Fig. 11. Motion control of the microrobot and *XY* stage is based on PID position control.

D. XY Stage Position Control

Under 40× magnification, the number of cells in one field of view is limited (∼10). The Petri dish bottom surface is 'virtually' divided into many adjacent rectangular segments, with each segment corresponding to one field of view in the image. Microinjection is conducted from segment to segment. The target position, P_d in the X_t-Y_t plane for the *XY* stage (Fig. 11) corresponds to the physical size of a segment, which is determined by the image size and calibrated pixel sizes.

V. Experimental Results and Discussion

A. Materials

The cells used in the experiments were primary porcine aortic endothelial cells, isolated from porcine aorta and cultured in cell medium (M199 medium, 5% calf serum, and 5% fetal bovine serum with a pH value of 7.4). Microrobotic injection was performed after 2 or 3 days of cell passage.

During system testing, both fluorescent dyes (dextran, Texas Red, 70,000 MW, neutral, Invitrogen) mixed with PBS buffer and QDs coated with 40% octadecylamine modified poly(acrylic acid) (wavelength=586nm) with a concentration of 1μM were injected. The size of QDs with coating is 17.2±1.2nm.

B. Results and Discussion

The semi-automated microrobotic system injected a total of 1012 endothelial cells, demonstrating an operation speed of 25 cells/minute. Cytoplasm instead of nucleus was selected as injection destination for each cell. The injected cells were inspected under a fluorescence microscope (IX81, Olympus), excited by 540nm laser light and observed through a TRITC filter set. Visual inspection was conducted right after injection. Fig. 12 shows microrobotically injected endothelial cells under both bright-field (Fig. 12(a)) and fluorescence microscopy (Fig. 12(b)). The deposited fluorescent dyes (high-brightness) can be clearly observed in the cells. Normal cell morphology is maintained after injection.

To quantitatively evaluate the performance of the microrobotic adherent cell injection system, two measures were defined. (1) *Survival rate:* This measure is defined as the ratio between the number of live cells after injection and the total number of cells injected, essentially representing the severity and frequency of cell damage from injection. Based on the 1012 injected endothelial cells, the microrobotic injection system produced a survival rate of 96%, which was determined through Trypan blue exclusion testing of cell viability. (2) *Success rate:* This measure is defined as the ratio between the number of cells with materials successfully deposited inside the cell and the total number of injected cells. Essentially, this measure represents the reliability and the reproducibility of the system. Visual inspection revealed that the success rate of the 1012 injected endothelial cells was 82%.

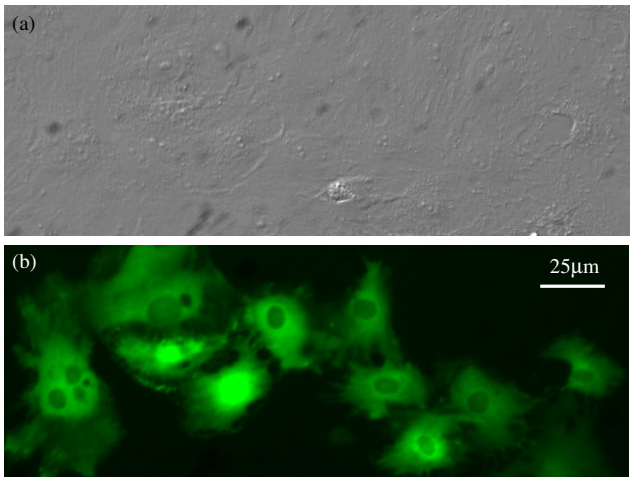

Fig. 12. Cells injected with fluorescent dyes. (a) Bright-field image showing normal cell morphology is maintained after injection. (b) Fluorescence microscopy image.

The semi-automated microrobotic system achieving an operation speed of 25 adherent cells per minute, a survival rate of 96% and a success rate of 82% compares favorably with manual injection. The system is immune from large variations in performance since efforts from operator intervention are trivial (computer mouse clicking) without causing human fatigue as in manual injection. Additionally, the system has a high degree of performance consistency, independent of proficiency differences across operators.

The 82% success rate implies that 18% of the injection operation failed to deposit materials into a cell, most probably due to the following two reasons: (1) The height/thickness variation across cells is significant. The vertical injection position of the micropipette tip was set at 3μm above the Petri dish surface for all cells. The lack of accurate knowledge on individual cell heights makes the system incapable of compensating for cell thickness variations. (2) More importantly, the surface flatness of commercial Petri dishes commonly used in a biology laboratory was found to often vary by 1-2μm even within a small neighborhood. Variations in surface flatness (i.e., unevenness) can cause the micropipette tip to either fail to enter a cell or penetrate through a cell. A substrate with more even flatness is expected to greatly alleviate this problem and further increase the success rate.

In the preliminary experiments of QD injection, the QD injected endothelial cells were cultured at 37°C in a CO_2 incubator and visually inspected under fluorescence microscopy. Fig. 13 shows the fluorescence images of two QD injected cells right after injection, 1hr after injection, and 2hr after injection. It appears that QDs gradually diffused throughput cytoplasm without entering the nucleus. Some QDs seemed

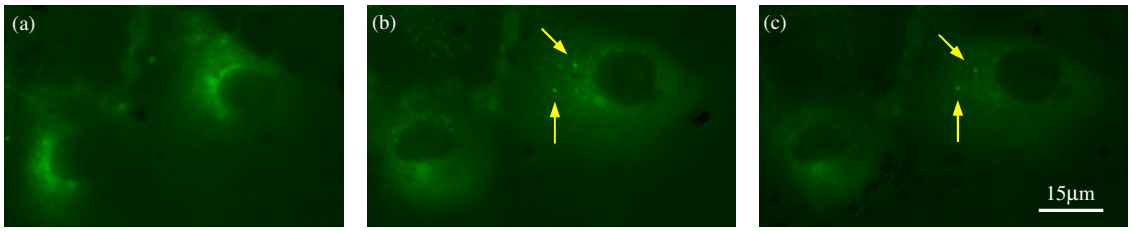

Fig. 13. Cells injected with QDs. (a) Right after injection. (b) 1hr after injection. (c) 2hr after injection. The aggregated QDs are labeled by arrows.

to form aggregates (arrow labeled in Fig. 13(b)(c)), possibly around specific organelles. In order to determine if QDs with a particular coating truly aggregate around an organelle in a selective manner, the next step requires us to selectively stain one organelle at a time and repeat the injection of QDs with different coatings into a large number of cells with the microrobotic adherent cell injection system. Detailed QD testing results will be reported later.

VI. Conclusion

The semi-automatic microrobotic system is capable of high-speed injection of adherent cells without requiring sophisticated operator skills. It experimentally demonstrated the capability of injecting 25 cells per minute and resulted in a survival rate of 96% and a success rate of 82%, based on the injection of 1012 endothelial cells during system testing. The computer vision microscopy based contact detection method automatically determines vertical alignment between the sub-micrometer micropipette tip and a cell with a high accuracy. For full automation, irregular cell morphologies must be robustly recognized through image processing in order to replace human intervention for selecting injection destinations. Significantly, the microrobotic system makes practical the injection of thousands of adherent cells within a short time window to enable large-scale molecule screening including our on-going research into the quantification of intracellular behavior of QDs.

Acknowledgment

This work was supported by the Natural Sciences and Engineering Research Council of Canada and by the Ontario Ministry of Research and Innovation.

References

[1] B. D. Chithrani, A. A. Ghazani, and W. C. W. Chan, "Determining the size and shape dependence of gold nanoparticle uptake into mammalian cells," *Nano Letters*, vol. 6, no. 4, pp. 662–668, 2006.

[2] N. Q. Jia, Q. Lian, H. B. Shen, C. Wang, X. Y. Li, and Z. N. Yang, "Intracellular delivery of quantum dots tagged antisense oligodeoxynucleotides by functionalized multiwalled carbon nanotubes," *Nano Letters*, 2007.

[3] A. Hoshino, K. Fujioka, T. Oku, S. Nakamura, M. Suga, Y. Yamaguchi, K. Suzuki, M. Yasuhara, and K. Yamamoto, "Quantum dots targeted to the assigned organelle in living cells," *Microbiology and Immunology*, vol. 48, no. 12, pp. 985–994, 2004.

[4] J. M. Klostranec and W. C. W. Chan, "Quantum dots in biological and biomedical research: Recent progress and present challenges," *Adv. Mater.*, vol. 18, pp. 1953–1964, 2006.

[5] W. J. Parak, R. Boudreau, M. L. Gros, D. Gerion, D. Zanchet, C. M. Micheel, S. C. Williams, A. P. Alivisatos, and C. Larabell, "Cell motility and metastatic potential studies based on quantum dot imaging of phagokinetic tracks," *Adv. Mater.*, vol. 14, no. 12, pp. 882–885, 2002.

[6] P. Scherp and K. H. Hasenstein, "Microinjection-a tool to study gravitropism," *Space Res.*, vol. 31, no. 10, pp. 2221–2227, Mar. 2003.

[7] Y. Sun and B. J. Nelson, "Biological cell injection using an autonomous microrobotic system," *Int. J. Robot. Res.*, vol. 21, no. 10-11, pp. 861–868, 2002.

[8] R. Kumar, A. Kapoor, and R. H. Taylor, "Preliminary experiments in robot/human cooperative microinjection," in *Proc. IEEE International Conference on Intelligent Robots and Systems (IROS'2003)*, 2003, pp. 3186–3191.

[9] L. Mattos, E. Grant, R. Thresher, and K. Kluckman, "New developments towards automated blastocyst microinjections," in *Proc. IEEE International Conference on Robotics and Automation (ICRA'2007)*, 2007.

[10] S. Zappe, M. Fish, M. P. Scott, and O. Solgaard, "Automated MEMS-based drosophila embryo injection system for high-throughput RNAi screens," *Lap Chip.*, vol. 6, no. 8, pp. 1012–1019, Aug. 2006.

[11] K. Schnizler, M. Kster, C. Methfessel, and M. Fejtl, "The roboocyte: automated (cdna/mrna) injection and subsequent (tevc) recording on xenopus oocytes in 96-well microtiter plates." *Receptors Channels*, vol. 9, no. 1, pp. 41–48, 2003.

[12] A. Pillarisetti, M. Pekarev, A. D. Brooks, and J. P. Desai, "Evaluating the role of force feedback for biomanipulation tasks," in *Proc. Symposium on Haptic Interfaces for Virtual Environment and Teleoperator Systems (HAPTICS'2006)*, 2006.

[13] W. H. Wang, X. Y. Liu, D. Gelinas, B. Ciruna, and Y. Sun, "A fully automated robotic system for microinjection of zebrafish embryos," *PLoS ONE*, vol. 2, no. 9, p. e862, Sept. 2007.

[14] P. J. Reddig and R. L. Juliano, "Clinging to life: cell to matrix adhesion and cell survival," *Cancer Metastasis Rev.*, vol. 24, pp. 425–439, 2005.

[15] G. L. Beretta, P. Perego, and F. Zunino, "Mechanisms of cellular resistance to camptothecins," *Curr. Med. Chem.*, vol. 13, no. 27, pp. 3291–3305, 2006.

[16] A. Kalota, S. E. Shetzline, and A. Gewirtz, "Progress in the development of nucleic acid therapeutics for cancer," *Cancer Biol. Ther.*, vol. 3, no. 1, pp. 4–12, Jan. 2004.

[17] A. M. Derfus, W. C. W. Chan, and S. N. Bhatia, "Intracellular delivery of quantum dots for live cell labeling and organelle tracking," *Adv. Mater.*, vol. 16, no. 12, pp. 961–966, June 2004.

[18] M. J. Lukkari, M. I. Karjalainen, R. Sarkanen, M.-L. Linne, T. O. Jalonen, and P. J. Kallio, "Electrical detection of the contact between a microinjection pipette and cells," in *Proc. The 26th International Conference (IEEE) Engineering in Medicine and Biology Society (EMBS'2004)*, San Francisco, Sept. 2004.

[19] W. H. Wang, X. Y. Liu, and Y. Sun, "Contact detection in microrobotic manipulation," *Int. J. Robot. Res.*, vol. 26, no. 8, pp. 821–828, Aug. 2007.

[20] D. L. Applegate, R. E. Bixby, V. Chvtal, and W. J. Cook, *The traveling salesman problem: A computational study*. Princeton University Press, 2006.